Jahn-Teller Dynamics in Charge-Ordered Manganites from Raman Spectroscopy

V. Dediu, C. Ferdeghini,* F. C. Matacotta, P. Nozar, and G. Ruani
Istituto di Spettroscopia Molecolare, CNR, via Gobetti 101, 40129 Bologna, Italy
(Received 8 October 1999)

The Raman spectra of the charge-ordered manganite $Pr_{0.65}Ca_{0.35}MnO_3$ were studied as functions of temperature and excitation energy and compared to magnetic moment and electrical conductivity behaviors. Both the charge ordering ($T_{co} \approx 225$ K) and the antiferromagnetic transitions ($T_N \approx 175$ K) affect the spectral shape and intensity, indicating strong charge-lattice and spin-lattice couplings. Below T_{co} a transition from dynamic Jahn-Teller distortions to a collective static distortion takes place. A change of the spectra is observed on increasing the excitation energy above 2.5 eV and it is attributed to a resonant polaron excitation.

PACS numbers: 75.30.Vn, 71.38.+i, 78.30.–j

Doped praseodymium manganites $Pr_{1-x}(Sr, Ca)_xMnO_3$ have the most unusual magnetic, electrical, and optical properties among the colossal magnetoresistance perovskites. The optimally doped Pr manganites ($x = 0.3$–0.5) are not ferromagnetic under usual conditions, showing insulating behavior down to low temperatures. Below ~230 K, charge ordering (CO) and orbital ordering take place, giving rise to a superstructure ($a' = 2a$) with the ordering of Mn^{3+} and Mn^{4+} cations along the a axis with one Mn^{4+}-O and two Mn^{3+}-O bond lengths [1].

$Pr_{1-x}(Sr, Ca)_xMnO_3$ is a Jahn-Teller (JT) system, where the JT distortion leads to a cubic-orthorhombic transition [2]. The JT distortion takes place on the Mn^{3+} sites, where the e_g level is twofold degenerate. The partial localization of the e_g electrons due to the JT effect or charge ordering is responsible for the "high" resistance values above the Curie temperature in manganites [3], while their delocalization leads to a ferromagnetic metallic phase via the double-exchange mechanism. Thus, the lattice-carrier coupling plays a crucial role to determine the magnetic and electrical properties of these manganites. Although the Raman spectroscopy is a powerful tool for studying such effects, the Raman spectra of manganites are not yet well understood.

In this Letter, we present the Raman spectra of $Pr_{0.65}Ca_{0.35}MnO_3$ single-phase polycrystalline samples along with their electrical and magnetic data across the charge-ordering transition, where structural, electrical, and magnetic properties change sharply.

The magnetization curve taken at 1 T by the SQUID magnetometer (Fig. 1) is in good agreement with available data [4] showing several features related to the magnetic and electrical transitions in this compound. A maximum below 250 K ($T_{co} \approx 225$ K from derivative analysis) indicates the charge-ordering transition, which leads to a strong carrier localization; a second maximum near 175 K coincides with the onset of antiferromagnetism (T_N), while a broad minimum above 100 K corresponds to the transition to canted spin order. These values are in good agreement with neutron diffraction data [5]. At low temperatures, a deviation from the canted spin behavior might be due to Pr-ion spin ordering [1].

Above T_N, the material is paramagnetic at both sides of the charge-ordering transition, but the nature of magnetic interaction changes drastically at T_{co}: It is ferromagnetic at $T > T_{co}$, with a Curie-Weiss behavior [$M \sim 1/(T - 160\ \text{K})$] and antiferromagnetic at $T < T_{co}$ [$M \sim 1/(T + 205\ \text{K})$]. The superexchange interaction, which competes with double-exchange interaction in the manganites [6], becomes dominant below T_{co} due to the strong carrier localization, driving the transition from a ferromagnetic to an antiferromagnetic interaction.

The resistance shows insulating behavior (inset in Fig. 1), with a sharp increase near T_{co}. Obviously, the Mn^{3+}-Mn^{4+} ordering decreases the frequency of the carrier hopping between the two manganese states.

Micro-Raman studies at different temperatures ($T = 4.2$–400 K) were recorded in backscattering geometry. Three different excitation energies were used in our studies: 488 nm (blue), 514 nm (green), and 632.8 nm (red).

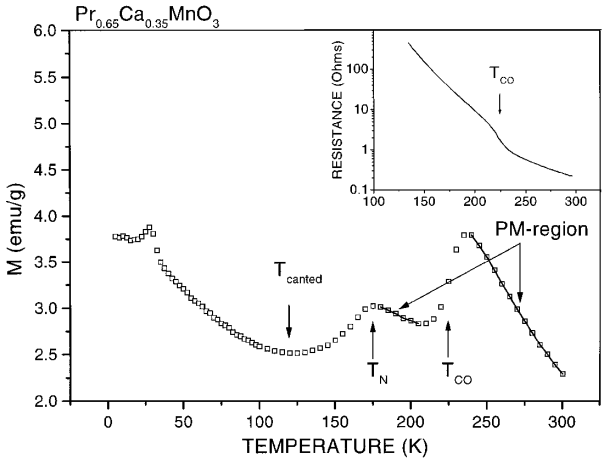

FIG. 1. Magnetization $M(T)$ curve measured at 1 T magnetic field. The solid lines near T_{co} are guides for the eye. The temperature dependence of electrical resistance is shown in the inset.

A 10× objective allowed us to collect the Raman spectra from sample areas of about 10 μm in diameter. As the spot is larger than the crystallite mean size (0.5–5 μm) we have not performed polarized measurements on polycrystalline samples. All the spectra recorded under the same experimental conditions at different positions of the samples were highly reproducible. Any set of data at a given temperature or excitation energy was taken precisely at the same position of the sample. Measurements at different power densities (15–650 W cm^2) have been performed for all the excitation energies. Except for the signal-to-noise ratios, no changes of the spectra were observed as a consequence of laser induced heating. Also, no photodegradation of samples was detected as a result of application of different excitation frequencies.

The Raman spectra excited with 632.8 nm photons at different temperatures are shown in Fig. 2. On top of a broad background that vanishes above 800 cm^{-1}, a few large peaks are observed at about 80 cm^{-1}, 145 cm^{-1} (ω_1), 475 cm^{-1} (ω_3), and 610 cm^{-1} (ω_4). From room temperature down to T_{co} no relevant variation in the spectra was recorded. Below T_{co}, the ω_3 and ω_4 peak intensities strongly increase. The two peaks become sharper and two new components ω_{3a} and ω_{4a} appear in the spectrum as sidebands at slightly higher energies. Similar peak "splitting" has been observed in nickelates at the charge-ordering transition [7,8]. Additionally, a new peak at 230 cm^{-1} (ω_2) becomes clearly visible and gains intensity lowering the temperature. On the contrary, the peaks at 80 and 145 cm^{-1} do not show any significant temperature dependence.

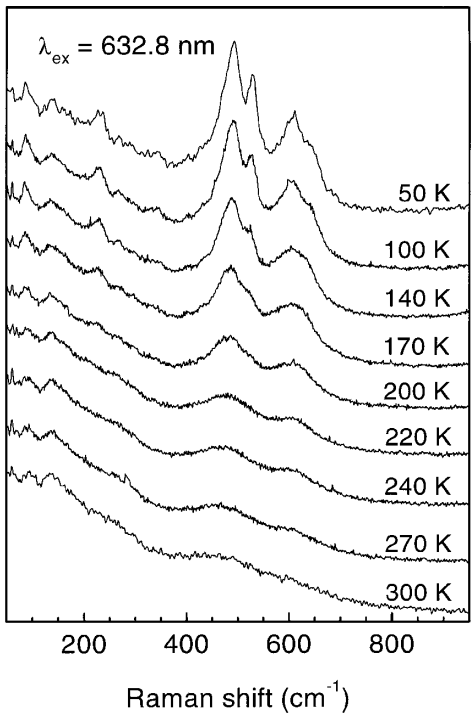

FIG. 2. Raman spectra excited with 632.8 nm at different temperatures. The intensity is given in arbitrary units.

Polarized Raman spectroscopy on related compounds [9] assigns the ω_3 and ω_4 modes to the apical oxygen bending A_g and the in-plane oxygen stretching B_{2g} in the MnO_6 octahedra. In particular, B_{2g} is one of the frozen phonons that form the JT distortion [10,11]. The temperature dependencies of peak energy, intensity, and half-width for the ω_3, ω_{3a} and ω_4, ω_{4a} bands were analyzed by fitting data with four Lorentzians (above T_{co}, four Lorentzians fitting gives two frequencies only: ω_3 and ω_4). The results are reported in Figs. 3(a), 3(b), and 3(c), respectively. The intensity transition below T_{co} mentioned above is now well resolved [Fig. 3(b)], as well as the peak splitting [Fig. 3(a)].

The appearance of the two sidebands ω_{3a} and ω_{4a} and of the ω_2 band below T_{co} can be explained by the lowering of the symmetry as a result of unit cell doubling along the a axis [1]. The folding of the Brillouin zone can determine the appearance of new Raman active Γ-point phonons [8]. Preliminary polarized Raman measurements on epitaxial films of $Pr_{0.65}Ca_{0.35}MnO_3$ at low temperatures indicate an

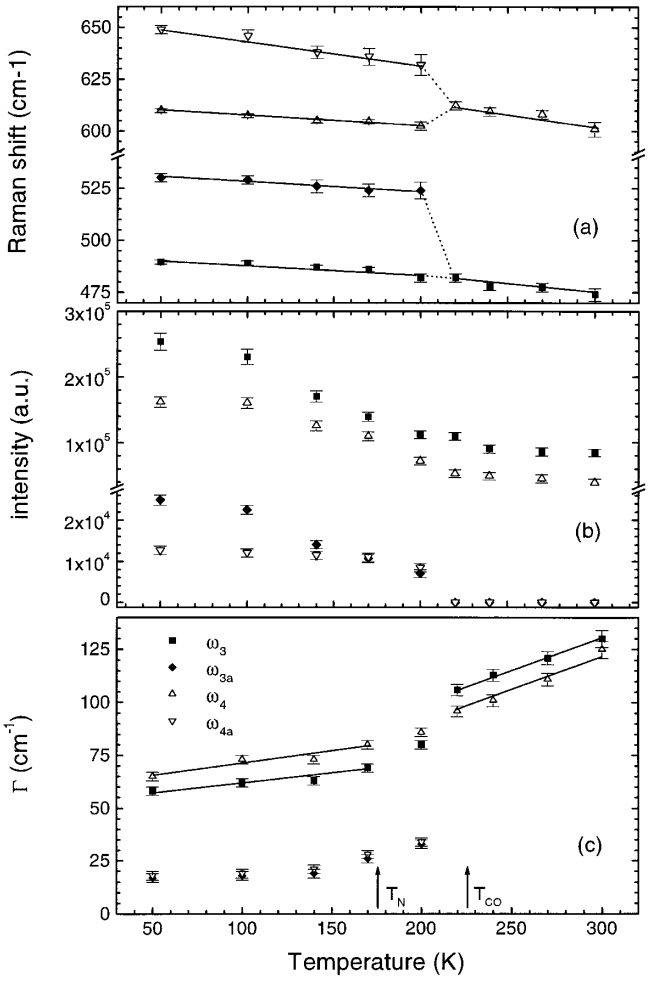

FIG. 3. The temperature dependencies of (a) peak energy (cm^{-1}), (b) integrated intensity (arb. units), and (c) width at half maximum Γ (cm^{-1}) of ω_3, ω_{3a}, ω_4, and ω_{4a} modes. Data were obtained by fitting the Raman spectra reported in Fig. 2 with four Lorentzians.

A_g character for the ω_3 and ω_{4a} peaks and a B_g character for the ω_4 and ω_{3a}.

In our opinion, the intensity increase of the ω_3 and ω_4 peaks below T_{co} is due to an order-disorder transition from dynamic JT to a static, cooperative JT effect. Above T_{co}, the JT distortion of the MnO_6 octahedra is averaged out by the fluctuation between Mn^{3+} and Mn^{4+} states due to a finite exchange hopping rate of the e_g electrons. Below T_{co}, the formation of charge-ordered domains leads to a static or quasistatic orthorhombic distortion where the electron hopping rate is strongly decreased. The large transition width indicates a gradual growth of the static domain fraction.

The half-width $\Gamma(T)$ dependencies for the ω_3 and ω_4 bands are rather similar, showing linear behavior at high and low temperatures, while the transition region is limited by T_N and T_{co} [Fig. 3(c)]. The narrowing of these bands is stronger below T_{co}, where the separation in two components takes place, while below T_N the saturation is observed. The difference in the half-width of the two components, ω_{3a} and ω_{4a} with respect to ω_3 and ω_4, can be due to the creation of charge-ordered stripelike domains in the system [12] and the possible differences in the coherence lengths of these structures in the directions parallel and perpendicular to the stripes.

The antiferromagnetic transition temperature coincides with the saturation point in Fig. 3(c). We believe that the antiferromagnetism in this structure is established once the long-range charge-ordered phase is built up. The reason for such a behavior is still to be understood. Nevertheless, it is reasonable to expect that the long-range cooperative magnetic interactions become possible only above a certain level of ordering in the mixed Mn^{3+}-Mn^{4+} system because of the anisotropic superexchange interactions associated with orbital ordering.

The folding of the Brillouin zone below T_{co} can also be responsible for the appearance of the ω_2 peak at 230 cm^{-1}. Nevertheless, we cannot rule out the assignment of this peak to the rotational soft mode of the MnO_6 octahedra mainly involving the apical oxygen atoms. This mode has been observed in the orthorhombic $La_{1-x}Sr_xMnO_3$ compounds in the same range of energy showing a characteristic temperature dependence [9,13].

Unusual results have been revealed by changing the excitation wavelength λ from 632.8 nm (1.5 eV) to 514 nm (2.4 eV) and to 488 nm (2.54 eV). Figure 4 shows the spectra taken using different excitation energies at a temperature (110 K) where the peaks are well resolved. The spectra have been normalized by taking into account the reflectance and the λ^4 scaling factor as well as the detector efficiency in the different spectral ranges. The spectra obtained by exciting with 514 nm are quite similar to those excited with 632.8 nm (Fig. 2) except that the separation of ω_3 and ω_4 in two components is not resolved and the relative intensities of the peaks are changed. On the other hand, the excitation with 488 nm leads to a rather different spectrum. A new band is detected at 375 cm^{-1} and the absolute intensity of the spectra is much larger with respect to the other two cases. The intensity of the ω_3 band, appearing as a small feature between the two bands at 375 and 635 cm^{-1} (ω_4), keeps the same order of magnitude, while the ω_4 band intensity increases roughly 5 times compared to the lower energy spectra. It is important also to note the strong change of the background with excitation energy.

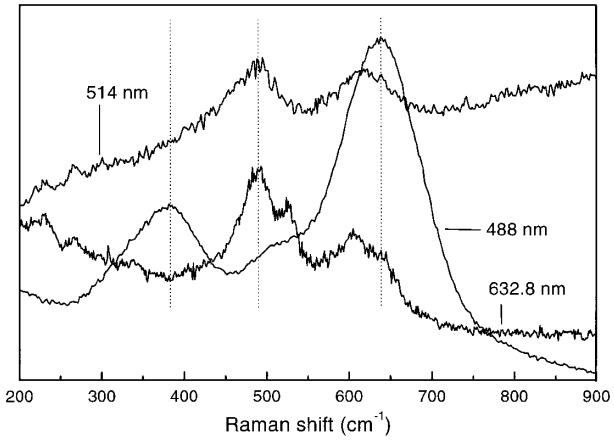

FIG. 4. Raman spectra excited with $\lambda = 632.8$, 514, and 488 nm at 110 K. The intensity has been normalized taking into account the efficiency of the CCD array detector, the λ^4 factor, and the material reflectance.

Except for a scale factor, the temperature dependence of the ω_4 peak intensity for the 488 nm excitation is similar to the one reported in Fig. 3(b), suggesting that the peak has to be associated with the same phonon mode. Although the peak does not reveal a clear splitting in two components below T_{co}, as observed on exciting with 632.8 nm, the weak softening of this peak at low temperatures can be explained by a change of the relative weight of the nonresolved ω_4 and ω_{4a}.

The peak at 375 cm^{-1}, which is nearly absent at room temperature, also shows a strong intensity enhancement below T_{co}. As mentioned before, we have not observed any excitation power dependence of the spectra in the explored range; moreover, the coincidence of the temperature at which Raman intensity changes and T_{co} makes us confident that no significant heating is induced by the laser. Consequently, the different spectra obtained with different excitation energies cannot be ascribed to thermal effects or photodegradation of the sample but should reflect different resonant conditions. While in principle the change of the background can be related to electronic Raman scattering, despite the narrowness of the electronic bands in $Pr_{0.65}Ca_{0.35}MnO_3$, it is hard to attribute an electronic nature to the intense sharp feature at 375 cm^{-1}. Processes like Raman active two-magnon [7] or orbiton excitation scattering [14] can also be ruled out as this mode is present also at room temperature.

We note that the strongest IR peak in the $Pr_{0.6}Ca_{0.4}MnO_3$ compound at 340 cm^{-1} [15] is close enough to the observed Raman band. In a crystal structure with center of inversion, infrared and Raman modes

are mutually excluded. However, local distortions like small polarons by breaking the symmetry can induce the activation in Raman of some IR active modes that can be amplified by resonance with the electronic levels associated with the local polaronic distortion. Therefore it is reasonable to assign the peak at 375 cm^{-1} to a resonant scattering with an IR derived mode associated to polaronic deformation. It has been shown that photogeneration of a large number of itinerant polarons with relatively large lifetimes leads to a metal-insulator transition in this system, with a maximum in the change of reflectivity at about 2.5 eV [16]. During the Raman measurements the density of photogenerated polarons should be too low for establishing a metallic state but can be high enough for providing a significant intensity of the induced non-Raman mode under resonant enhancement. These results emphasize once again the important role polarons seem to play in manganese as well as copper perovskites [17]. Polaronic excitations have been theoretically predicted [18] and observed in manganites in a large variety of experiments, including resistivity [19], thermopower [20], and optical measurements [21].

In conclusion, the charge ordering in $Pr_{0.65}Ca_{0.35}MnO_3$ was detected by resistive and magnetic measurements and by micro-Raman spectroscopy. Strong charge-lattice and spin-lattice couplings were observed in this material. A transition from dynamical JT to static JT distortion was detected below the charge-ordering transition temperature. New Raman active Γ-point phonons appear below T_{co} due to the folding of the Brillouin zone. The effect of resonant polaron excitation is supposed to be responsible for a noticeable change of the Raman spectra excited with 2.54 eV (488 nm) radiation.

We thank J. B. Goodenough for very useful discussions.

*INFM-Università di Genova, Dipartimento di Fisica, via Dodecaneso 33, 16146 Genova, Italy.

[1] D. E. Cox, P. G. Radaelli, M. Marezio, and S.-W. Cheong, Phys. Rev. B **57**, 3305 (1998).
[2] A. A. Elemans, B. van Laab, K. R. Van der Veen, and B. O. Loopstra, J. Solid State Chem. **3**, 238 (1971).
[3] A. J. Millis, Nature (London) **392**, 147 (1998).
[4] M. R. Lees, J. Barrat, G. Balakrishnan, D. McK. Paul, and M. Yethiraj, Phys. Rev. B **52**, R14 303 (1995).
[5] Y. Tomioka, A. Asamitsu, H. Kuwahara, Y. Moritomo, and Y. Tokura, Phys. Rev. B **53**, R1689 (1996).
[6] P.-G. DeJennes, Phys. Rev. **118**, 141 (1960).
[7] K. Yamamoto, T. Katsufuji, T. Tanabe, and Y. Tokura, Phys. Rev. Lett. **80**, 1493 (1998).
[8] G. Blumberg, M. V. Klein, and S.-W. Cheong, Phys. Rev. Lett. **80**, 564 (1998).
[9] M. N. Iliev, M. V. Abrashev, H.-G. Lee, V. N. Popov, Y. Y. Sun, C. Thomsen, R. L. Meng, and C. W. Chu, Phys. Rev. B **57**, 2872 (1998).
[10] M. V. Abrashev, A. P. Litvinchuk, M. N. Iliev, R. L. Meng, V. N. Popov, V. G. Ivanov, R. A. Chakalov, and C. Thomsen, Phys. Rev. B **59**, 4146 (1999).
[11] S. Satpathy, Z. S. Popovic, and F. R. Vukajlovic, Phys. Rev. Lett. **76**, 960 (1996).
[12] S. Mori, C. H. Chen, and S.-W. Cheong, Nature (London) **392**, 473 (1998).
[13] J. C. Irwin, J. Chrzanowski, and J. P. Franck, Phys. Rev. B **59**, 9362 (1999).
[14] V. Perebeinos and P. B. Allen, e-print cond-mat/9906118.
[15] Y. Okimoto, Y. Tomioka, Y. Onose, Y. Otsuka, and Y. Tokura, Phys. Rev. B **59**, 7401 (1999).
[16] M. Fiebig, K. Miyano, Y. Tomioka, and Y. Tokura, J. Appl. Phys. **85**, 5561 (1999).
[17] K. A. Muller, J. Supercond. **12**, 3 (1999), and references therein.
[18] A. J. Millis, B. I. Shraiman, and R. Mueller, Phys. Rev. Lett. **77**, 175 (1996).
[19] M. Ziese and C. Srinitiwarawong, Phys. Rev. B **58**, 11 519 (1998).
[20] M. Jaime, M. B. Salamon, M. Rubinstein, R. E. Treece, J. S. Horwitz, and D. B. Chrisey, Phys. Rev. B **54**, 11 914 (1996).
[21] K. H. Kim, J. H. Jung, and T. W. Noh, Phys. Rev. Lett. **81**, 1517 (1998).